Translating Phased Array Measurements of a Low-Noise Top-Mounted Propulsion Installation for a Supersonic Airliner

JORDAN CLUTS[*], JAMES BRIDGES[*†], GARY PODBOY[*]
NASA Glenn Research Center, Cleveland, OH 44135

A novel translating-phased-array technique was applied during a model-scale validation test of low-noise propulsion concepts for supersonic transport aircraft. Data were acquired for a series of nozzles with different chevron designs, both uninstalled and installed on a representative aircraft planform. The far field data confirmed the noise reduction potential of top-mounted installation, while the phased array results gave insights into how the reduction occurred and highlighted areas for improvement. This was the inaugural test for the new translating phased array, which measures source maps as seen by observers at different polar angles. Propagation effects through the free jet were documented for the different viewing angles. The source maps obtained were used to understand important aspects of the far field noise measurements.

I. Introduction

In previous model testing[1] a greater acoustic effect was found from installation than from nozzle type for a given engine. In the concept vehicle studied, one center engine was mounted above the aft deck of the aircraft while two outboard engines were mounted below. The propulsion system mounted on the top of the aircraft had substantial (2-3 EPNdB) shielding of mixing noise in the frequency range of peak human annoyance. The propulsor mounted under the aircraft body experienced a substantial increase (again 2-3 EPNdB) in noise due to reflection of the mixing noise from the underside of the aircraft. Based on this result, NASA explored the noise reduction that could be obtained by moving both outboard propulsors to the top of the concept vehicle, and estimated the possible acoustic advantages and aerodynamic impacts on range and sonic boom. The results were promising, estimated at 4-5 EPNdB reduction of the jet mixing noise and totally eliminating the contribution of fan noise in the EPNdB calculation.

Chevrons and other mixing enhancement features of a nozzle usually increase turbulent mixing near the nozzle while reducing the jet velocity and turbulence downstream. This has been used to reduce the peak, low-frequency jet noise directed at aft angles. However, the enhanced mixing increases the high frequency sound, which is at peak annoyance to humans, as the increased turbulent mixing energy close to the nozzle creates more noise. Balancing the benefit of reducing the low with the penalty of enhancing the high frequencies so that humans perceive the result to be less annoying has been the challenge of designing such nozzles. Given that enhanced mixing usually decreases thrust further adds to the difficulty.

However, installation effects allow us to break this benefit/penalty dilemma. If the enhanced-mixing nozzle is mounted on the top of the vehicle, the enhanced high frequencies can be shielded from the observer while the uncovered low frequencies downstream will be reduced. If the mixing is brought far enough upstream and the noise adequately shielded the result will be a large reduction in annoyance to the observer. The key is accurately predicting the distribution of noise sources at different frequencies to produce the maximum benefit, while maintaining adequate aerodynamic performance of the nozzle.

To explore this concept, a simplified acoustic analogy code for predicting jet noise was employed on an exhaust system studied previously with conventional, underbody installation[1,2]. The previously tested inverted velocity

[*] Acoustics Branch,
[†] AIAA Associate Fellow

profile (IVP) exhaust system, featuring a tertiary stream over a 180° annulus, was used as the baseline nozzle. The previous concept aircraft was then reimagined with all top-mounted propulsion as shown in Figure 1, and chevron nozzles were designed to shift the noise sources upstream to obtain greater suppression than the unenhanced, baseline nozzle. The chevrons were designed to augment mixing between the primary and flight streams, between the primary and tertiary streams, and between the tertiary and flight streams. A planform representation of the airframe was created to mimic the installation of the propulsion units on the top of the vehicle. Combinations of the nozzle, chevrons, and planform allowed evaluation of system-level estimates of noise reduction for the installation of the baseline nozzle, and exploration of the additional benefits of modifying noise source distributions.

Tests were conducted using various measurement systems to fully characterize the jet plume and its noise. Noise source distributions measured with a phased array are presented in this paper. Companion papers are also being presented at this conferenced including: measurements of the far field sound[3], particle image velocimetry of the jet plume[4], and computational work using Reynolds-Averaged Navier-Stokes[5]. Collectively this work describes the jet plume, noise sources, and radiated sound that can be expected from this configuration.

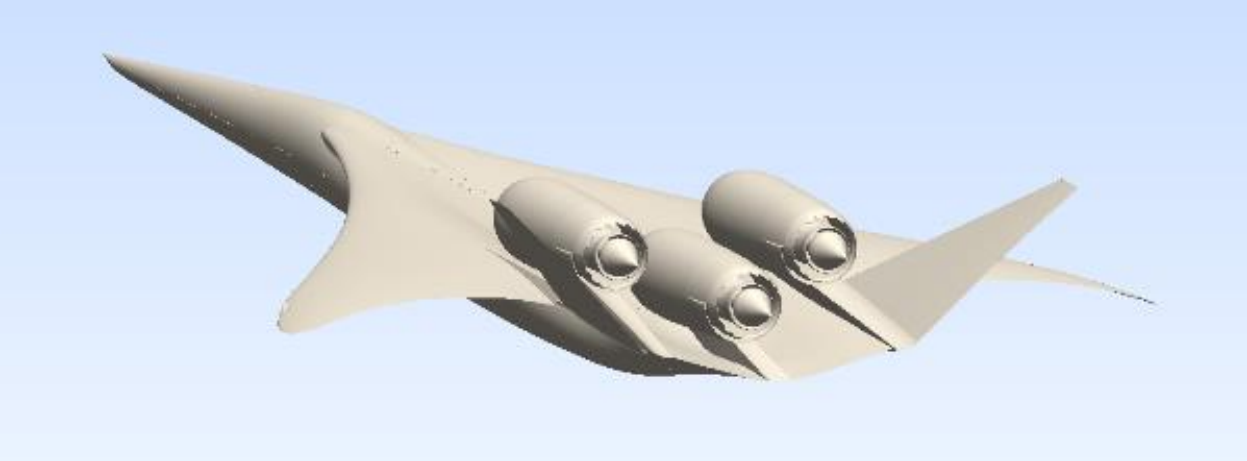

Figure 1 Concept aircraft with three top-mounted, podded engines.

II. Facility and Instrumentation

The test was conducted in the NASA Glenn Research Center AeroAcoustic Propulsion Laboratory (AAPL). The AAPL is a 19.8 m (65 ft) radius anechoic geodesic hemispherical dome. Acoustic wedges cover the walls of the dome and approximately half of the floor area. The AAPL was acoustically clean for all acoustic test runs, with acoustic wedges on the front and microphone sides of all surfaces of the facility. The ambient temperature, pressure, and relative humidity were recorded within the dome during each data acquisition and used to transform the data to standard day conditions (ISA +10).

The Nozzle Aeroacoustic Test Rig (NATR) is contained in the AAPL. The NATR provided the flight stream for the jet rig. The NATR ductwork was acoustically lined on both the inside and outside and consisted of an annular ejector system connected to a plenum followed by the transition section which was an ASME long-radius, low-beta venturi nozzle. The NATR flow was exhausted through a 1.35 m (53 in) diameter nozzle to form a free jet to simulate the effects of forward flight on the test article. The centerline of the free jet was 3.05 m (10 ft) above the floor. An acoustically treated wall separates the NATR from the section of the building which did not have acoustic treatment on the floor, preventing unwanted reflections from the both the untreated floor area and adjacent test equipment.

The High Flow Jet Exit Rig (HFJER), located at the downstream end of the NATR, is the structure through which heated air was delivered from the facility compressed air system to the test article. The HFJER is effectively a turbofan engine simulator. The first air stream can be heated up to 427° C (800° F) using a natural gas, with pressure ratios up to 2.6. The second air stream can be heated up to 54° C (130°F) using a heat exchanger at pressure ratios up to 2.0. The combined mass flow of the two streams cannot exceed 13.6 kg/sec (30 lbm/sec). For this test, HFJER was fitted with a third annular stream of air to feed three-stream, variable cycle nozzles. This third stream, which

was diverted from the usual second stream prior to its control valve, was independently controlled for pressure but shared roughly the same temperature as the second stream.

The rig, depicted in Figure 2, was fitted with a rotating collar section downstream of the third-stream plenum. A support arm cantilevered downstream from the outer rotating spool of the rotating collar section to support the model planforms and allow them to be positioned at multiple azimuthal angles. Next on the stack was a stream invertor (labeled "IVP adapter" in Figure 2) that ducted the second annular airstream into the center of the nozzle system, producing the inverted velocity profile capability. The nozzle model hardware, described below in detail, attached to this stream invertor. Rotations of the model system, both nozzle and planform, were relative to the far field array, ~30° counterclockwise from vertical in AAPL. The rig was instrumented to record total temperature and total pressure at the charging station on all streams, including the IVP-specific instrumentation in the cold stream of the inner flow path. In addition, mass flowrates were recorded using flow venturi. Ambient conditions were recorded on the facility computer, along with all rig instrumentation, at a 1 Hz sample rate during periods of acoustic data acquisition. Relative humidity and temperature were recorded both at 3.05 m (10 ft) above the floor near the NATR and near the top-most region of the overhead microphone array, located roughly 18.3 m (60 ft) above the floor. Ambient pressure was recorded in a sheltered location within the dome.

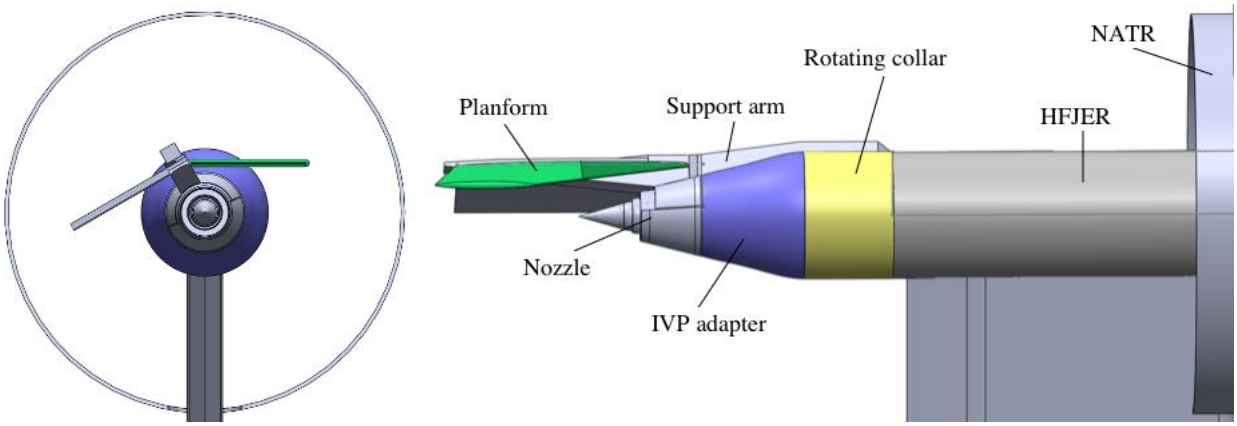

Figure 2 Rig and model hardware, with components identified.

Translating Phased Array

A phased array was developed for this test to measure the source distributions from different polar angles. The phased array has 48-microphones logarithmically spaced along 5 spiral arms. The array is a 60% scale of the original Array48 design marketed by OptiNav Inc. (the microphone pattern was licensed from OptiNav for this application). The microphones are low-profile GRAS 47BX microphones, flush mounted on the surface of a 0.75 m (29.5 in)-diameter disk. A video camera was mounted in the center of the array to provide optical registration of the phased array results. The microphone signals were recorded by a Genesis GEN3i data recorder at 200 kHz sample rate and processed using OptiNav's ImageJ-based processing software, Beamform Interactive.

The phased array deployment was significantly different than that of the OptiNav Array48 system previously used at AAPL. The new array was mounted on a mast and rotating stage which in turn was mounted atop an 8.7 m (28.5 ft) long linear traverse. Both the rotating stage and linear traverse were remotely operated. The rotating stage allowed the array normal axis to be aimed at angles between +90° and -90° relative to a line perpendicular to the linear traverse. This linear traverse was positioned on the floor of the AAPL parallel to the jet axis at a distance of 2.0 m (6.5 ft) from the centerline and the array was mounted at an elevation 3.0 m (10 ft) above the floor (level with the jet centerline). The layout is diagramed in Figure 3. As illustrated, the combination of the linear traverse and the rotating stage allowed the phased array to be moved between polar angles of 30° and 150° relative to the upstream jet axis. The array was installed and operated to have the array's normal vector oriented at a point on the jet axis and 0.50 m (19.5 in) downstream of the nozzle plug tip. This was chosen to be the middle of the field of view, assuming that the source distributions would extended from the nozzle exit to 1 m downstream. Several stations were defined for measurements to be taken at, primarily 60°, 90°, and 135° polar angles although other stations were tested as well. The phased array remained stationary while measurements were taken. It was then repositioned remotely to take a measurement at a different station, allowing for different measurements of the same flow conditions.

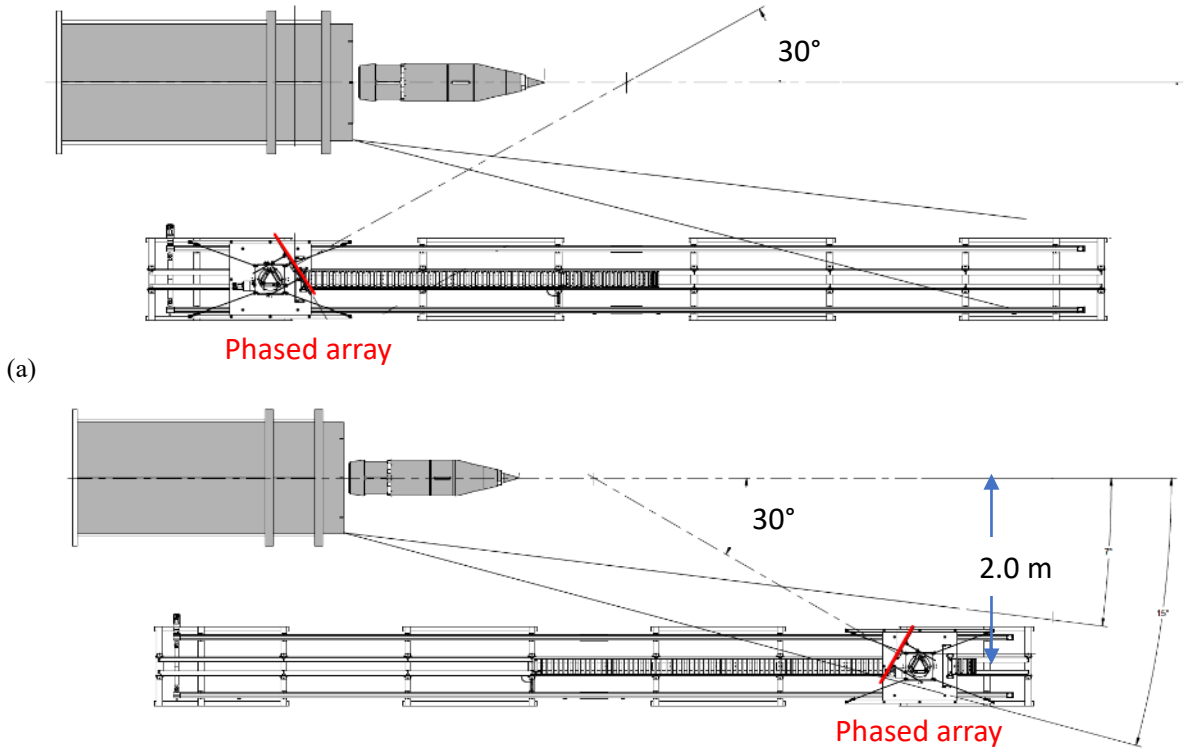

Figure 3 Installed geometry of the translating phased array, top view. NATR and HFJER shown in grey, and array positioned in extreme (a) upstream and (b) downstream locations.

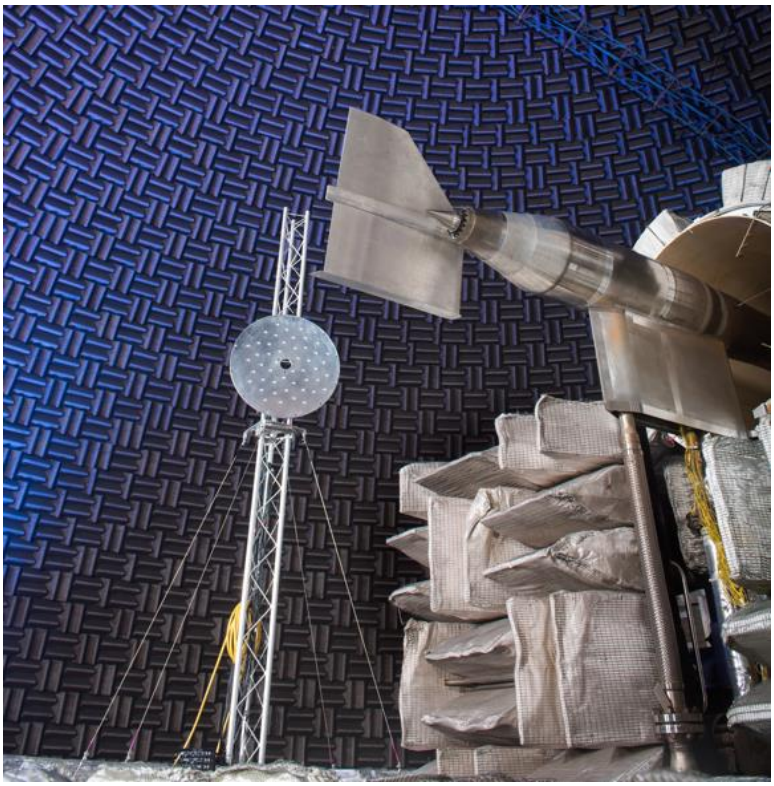

Figure 4 Photo of translating phased array positioned at upstream location.

Beamforming algorithms

Beamforming algorithms were used to process the data provided by the phased array. A phased array consists of multiple microphones for which the position in space of each microphone is accurately known. Using the acoustic signals of each of the microphones in concert with the positional information of the microphones relative to the region of interest, beamforming algorithms determine the acoustic source strength at different locations in the region of interest. All beamforming algorithms generate sidelobes, weaker false acoustic peaks arrayed around each actual sound source generated by the multitude of phases that align with the finite number of microphones in the array. Sidelobes can be reduced by positioning the microphones in configurations that prevent even overlap of the phase difference between different microphones, often done using a logarithmic spiral. This positioning, however, does not eliminate sidelobes and their presence can make it difficult to identify multiple sound sources in a given region of interest as they may be confused for a sidelobe of another source. Different beamforming algorithms have been developed in an attempt to reduce and filter sidelobes in the beamforming map.

Three different beamforming algorithms were explored, Conventional Frequency Domain Beamforming, Functional Beamforming and High-Definition Beamforming. Conventional Frequency Domain Beamforming, also known as delay and sum beamforming, is the original beamforming algorithm. The algorithm analyzes the signal from each of the microphones and determines the position of a noise source using the arrival time of the acoustic signals at the different microphones. This is accomplished efficiently by using an intermediate representation called the Cross Spectral Matrix or CSM. The CSM represents the degree of correlation between every combination of microphones at every frequency of interest. It encapsulates all the acoustic information needed for beamforming. Conventional Beamforming is relatively fast but produces relatively strong sidelobes and a relatively broad spatial representation of a noise source, i.e. a noise source normally appears larger in the beamform map than it actually is. The other methods explored use more advanced processing techniques to suppress the sidelobes that conventional beamforming creates as well as to increase the effective spatial resolution of the phased array, more precisely indicating the size and position of noise sources in the region of interest.

Functional beamforming, is a technique that modifies the CSM using a freely chosen parameter to improve the beamforming performance[6]. The CSM is raised to the inverse of the chosen parameter. Conventional Beamforming is then applied to this modified CSM. Finally, the resulting beamforming map is raised to the power of the free parameter. This has the effect of preserving the power in the strongest peak, while reducing sidelobes and thereby sharpening sources.

Lastly High-Definition Beamforming is explored. This is a proprietary algorithm created by Opti-Nav.

III. Model Hardware

Model hardware configurations

The installed exhaust concepts being evaluated in this test program consisted of nozzles installed above aft decks of the aircraft with variations in an enhanced mixer to shift the noise sources further upstream for increased shielding. A baseline (no chevrons) nozzle and several mixing enhanced nozzles were tested. The mixing enhanced nozzles employed chevrons to shift noise sources upstream.

Nozzle: The baseline nozzle had three streams and an external plug. The inner annulus is axisymmetric and thin, carrying approximately half the flow generated by the three-stream engines' tip fan. The second annulus is the primary stream, passing the core and primary fan streams which would be fully mixed upstream in the conceptual engine. It is also axisymmetric. The tertiary nozzle carries the other half of the tip fan flow, and is an annulus that covers roughly half of the circumference of the nozzle. This tertiary stream makes the plume bisymmetric, and requires a notation as to whether the observer is on the side facing the tertiary stream, denoted as 'A0', or away from it, denoted as 'A180'.

Chevrons: Chevrons were installed on the nozzles for mixing enhancement. The location and penetration of the chevrons varied. Chevrons were applied to a 180° arc over either side of the primary nozzle. The nomenclature of these locations is given in Figure 5. Two chevron designs, differing in penetration but having the same length and number (eight), were tested. The two designs were approximately the same on each side, with a set of lower penetration chevrons having an angle 10° to the centerline, and a higher penetration design having an angle of 16° to the centerline. Thus, two chevron designs could be deployed independently on either side of the primary nozzle.

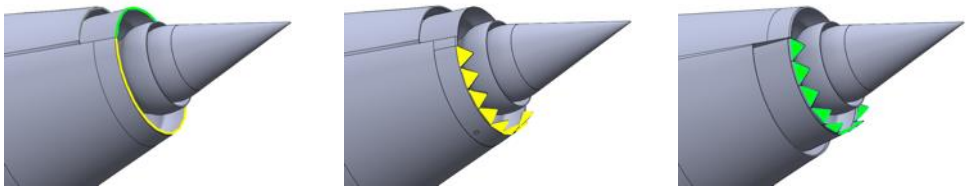

Baseline nozzle Primary-flight chevrons Primary-tertiary chevrons

Figure 5 Nomenclature for locations of chevrons. Note that exhaust system is rotated between views.

Collectively, the hardware allowed a number of parameters to be varied, including chevron location, chevron penetration and planform shape. The codes used to describe the different configurations are enumerated in Table 1. In addition, the hardware allowed the azimuthal observation angle to be varied.

Table 1 Hardware Configuration Codes

Component Code	Description
000	Baseline lip insert
100	Low-penetration primary-flight chevrons
200	High-penetration primary-flight chevrons
040	High-penetration primary-tertiary chevrons
B	No planform
T	Installed with planform

Impinging jet noise source

It is important to use a known noise source to register the phased array, ensuring that pixels in the beamform map correspond to the same locations in space as those of the optical camera. One source used in this process was the impinging jet, shown in Figure 6. The jets were supplied with a 100 psi (shop air) source and the resulting impinging jets produced a relatively loud broadband source. This source was loud enough to be used while the free jet was in operation, and was used to determine the spatial shift produced by the sound propagating across the free jet.

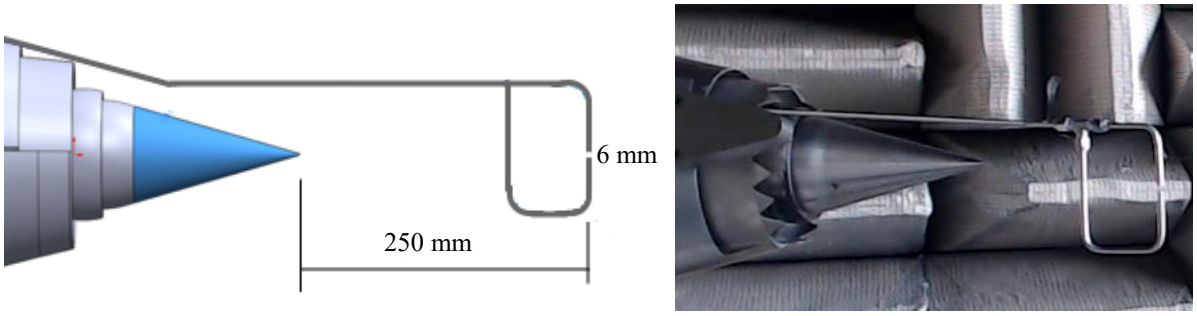

(a) *(b)*

Figure 6 Geometry of impinging jet source. 6 mm (0.24 in) gap between nozzles located 250 mm (9.8 in) downstream of nozzle plug. (a) as designed, (b) photo of implementation.

IV. Flow conditions

The flow conditions were defined from cycles studied under the NASA Low-Noise/Low-Boom Tech Challenge[7]. In that study, a three-stream (tip-fan) engine was defined that, when installed on a conceptual supersonic aircraft, met the ICAO Chapter 14 airport noise regulations when programmed lapse rate was implemented. The inverted profile nozzle achieved an acceptable noise level when installed in the two engines-below, one engine-above configuration when the engines were running at a primary nozzle pressure ratio of 1.86. In the conceptual engine, the primary stream of the nozzle was fed by mixing the core and main fan streams internally, producing a mixed temperature around 555 °K (1000 °R) at a pressure ratio of 2, and the tertiary fan stream, split between the innermost and tertiary nozzle passages was operating at a pressure ratio roughly 1.8 and temperature of 361 °K (650

°R). For the translating phased array portion of this test, the cycle was defined over the pressure ratio range from 1.8 to 2.3. The flight stream was M_{flight} = 0.3 for all test points.

V. Results

Translating Phased Array and Beamforming Algorithm Evaluation

The first test objective was to show how well the phased array could resolve an artificial noise source with known position in the NATR free jet. This was to be determined for different frequencies, polar angles, free jet speeds, and with different beamforming algorithms. In addition, the processing could be used to image the sources to an equivalent source distribution on a plane parallel to the phased array (parallel view) or on the streamwise plane colinear with the jet axis (streamwise view). In most phased array work involving jets, the phased array is located at a 90° polar angle such that a line normal to the phased array plate is also normal to the jet centerline. In such a case, the parallel and streamwise views are the same. For polar angles away from 90°, however, the projection onto the streamwise plane can be problematic, as will be shown below. Further complicating the beamforming is the effect of sound convection with the free jet stream.

The noise source used in this evaluation work was the impinging jet (Figure 6). The source maps in Figure 7 – 10, correspond to different methods of beamforming and different polar angles. Since the impinging jet source is approximately a point source, it should look similar from all angles. Different beamforming algorithms may change the spatial resolution, however, depending upon how the algorithm handles ideal sources and how it handles the phase distortion produced by the free jet turbulence.

Figure 7 shows source maps corresponding to no free jet velocity at 10 kHz. The data have been processed to show the sources on the streamwise plane passing through the jet centerline and are overlaid on top of a photo taken with the phased array camera at a polar angle 90° to the jet. The functional and high-def beamforming much more narrowly pinpoint the noise source compared with the relatively diffuse peak of the conventional beamforming. All three techniques accurately locate the noise source at 90° and 135° but at 60° they all locate the peak source upstream of its true position. Since there is no flow to account for this, the projection onto the 90° degree plane must be causing the inaccuracy.

Figure 8 shows the source map when the free jet flight stream is at M= 0.3 at 10 kHz. The data is now mapped to the parallel view. All of the maps are much more diffuse than the static case (Figure 7), but the maps for 135° are even more diffuse and are inaccurately locating the peak source. Here at 10 kHz, there is less difference between the beamforming algorithms than at other frequencies (not shown).

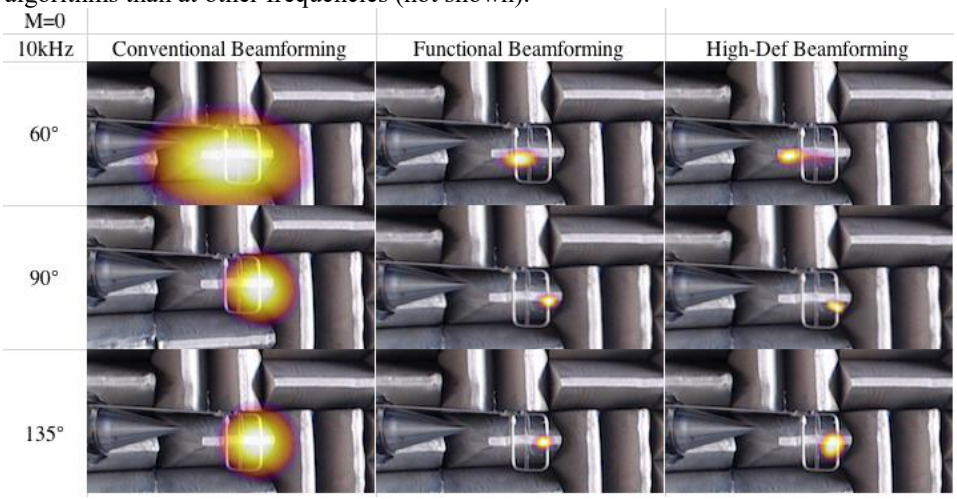

Figure 7 Source distribution of impinging jet as processed by three different beamforming algorithms at three polar angles, projected to the streamwise view. No flight stream, 10 kHz center frequency band.

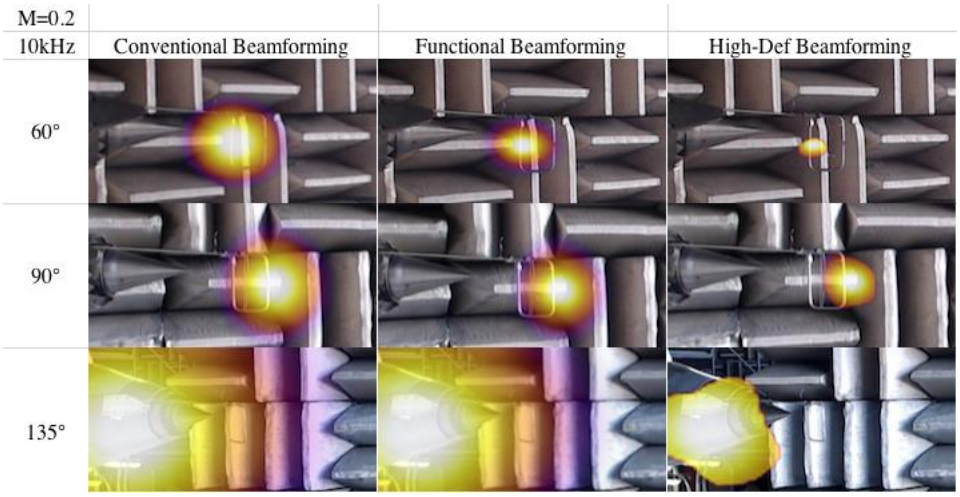

Figure 8 Source distribution of impinging jet as processed by three different beamforming algorithms at three polar angles, projected onto parallel plane containing the source. M=0.2 flight stream, 10 kHz center frequency band.

All the algorithms produced reasonable distributions when there is no flight stream, with the Conventional beamforming being much more diffuse than the other algorithms at all frequencies. Solving for sources on the jet streamwise plane caused some problems when the data was acquired at the 60°polar angle, but strangely did not cause an issue for the 135° polar angle. When the flight stream was active, all the source maps are more diffuse and all but the 90° polar angle were misplaced. The 135° maps, in particular, were nonsensical. The maps produced by Conventional beamforming were significantly more diffuse than others whereas the maps from High-Def beamforming were sometimes much less diffuse than the other algorithms but appeared to be inconsistent. The Functional beamforming algorithm produced consistent source maps and was chosen for use in further analysis.

To interpret noise source maps for jet flows in the presence of the flight stream, a 'spatial calibration' of the maps was required. The calibration discussed here involves determining how much a source appears to shift downstream at different flight speeds and assumes that all sources would shift the same distance regardless of where they are located in the jet. Consequently, it is not as precise as if the beamforming were done with steering vectors created to account for the refraction of the free jet (which would account for phase variations between microphones).

Figure 9 shows source distributions over a wide range of frequencies as determined at the three polar angles with no free jet velocity. The source region decreases in size rapidly with increasing frequency, but the peak location does not change with frequency. For each polar angle (column in the figure), a dashed line is drawn at the location of the source.

Figure 10 shows source distributions for the same frequencies and angles but at flight speed M = 0.3. For each polar angle, two dashed lines are drawn, one at the actual location of the source as determined from Figure 9 and one through the peaks of the source maps. There is a displacement between the actual source location (green) and observed location (black) for the M = 0.3 case.

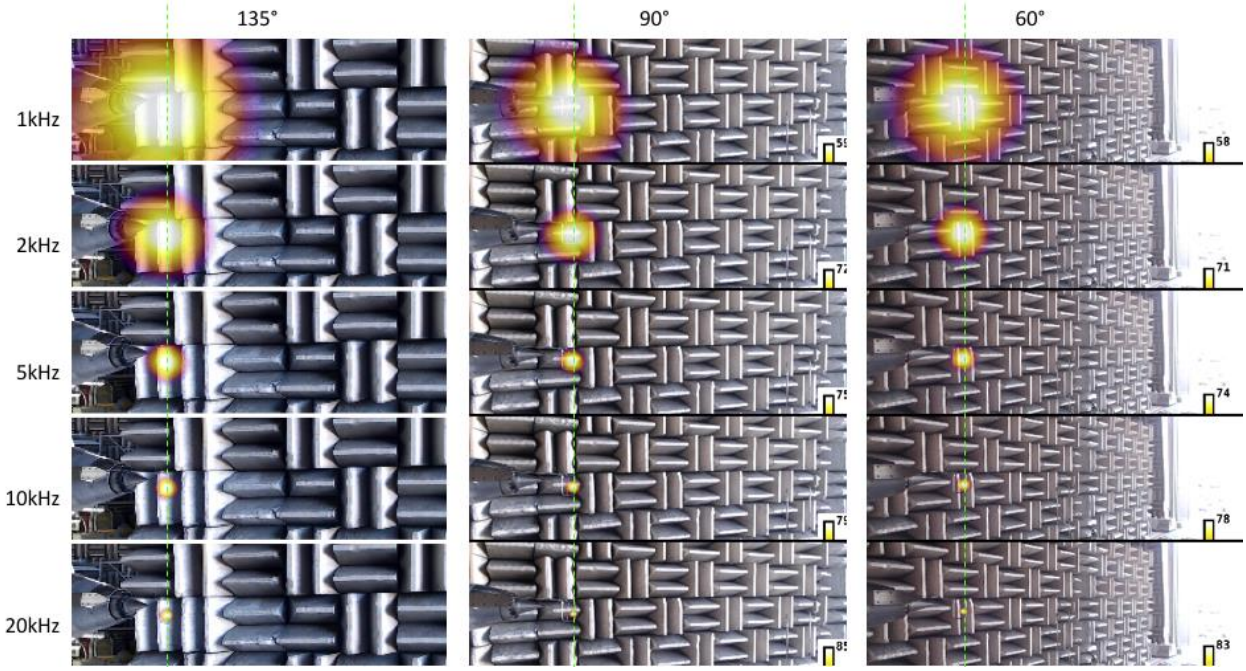

Figure 9 Source distributions for impinging jet as processed by Functional beamforming algorithm at three polar angles, projected onto parallel plane containing the source. Green dashed line marks location of actual source. M = 0 flight stream (no flow).

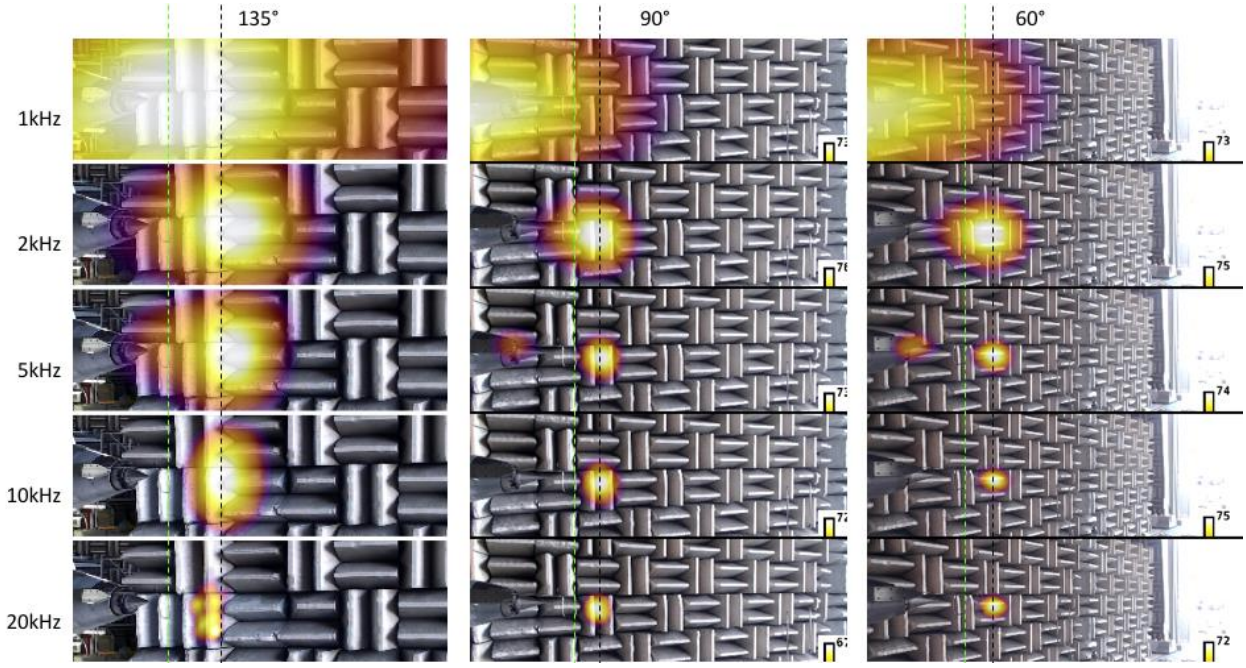

Figure 10 Source distributions for impinging jet as processed by Functional beamforming algorithm at three polar angles, projected onto parallel plane containing the source. Green dashed line marks location of actual source; black dashed line marks peak of source distribution. M = 0.3 flight stream.

A geometric explanation for the shift in apparent source location due to the change in viewing angle is illustrated in Figure 11. This shows the jet rig and nozzle mounted in the free jet with the phased array located at a downstream polar angle. Suppose that an actual source is located at the nozzle exit and we are interested in the waves emitted in the downstream direction, marked as 'Emitted'. The speed of the wavefront relative to the air is the speed of sound, but to a fixed observer, the component of propagation velocity in the downstream direction is augmented by the

convection speed of the free jet flow M_{flight}. The wavefront is therefore directed at an angle $\tan^{-1}(M_{flight})$ greater than the emitted angle until it leaves the free jet. The edge of the free jet is notionally shown here as a dashed line. Upon leaving the free jet stream the propagation velocity is again the same in all directions, however, the wavefronts now have a center of curvature downstream of the actual source location. Since the beamforming was done assuming spherical spreading in an ambient medium, the beamforming algorithm assigns the origin of the energy to the center of curvature of the wavefront, at the location of the apparent source. The sketches in Figure 12 show how this geometry changes with the different polar angles used in the present study, assuming a 3° shear layer growth rate for the free jet shear layer. Using these geometries, differences between the apparent and actual source locations were calculated for the three polar angles. The measured differences from Figure 10 and similar measurements at different flight speeds are plotted versus flight speed M_{flight} in Figure 13, and the expected differences from the calculations are included in the figure. The calculated shift agrees with the measured shift, confirming this explanation for the shift. The source distributions shown later in this paper have not been corrected for this displacement, but future data processing could adjust for this effect.

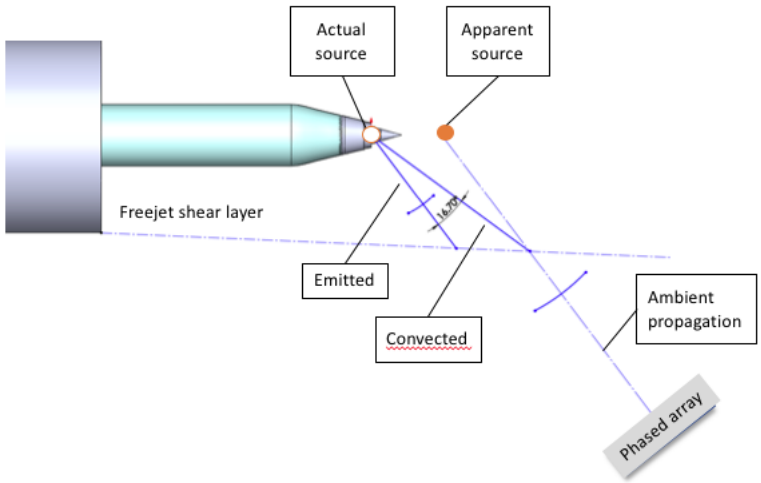

Figure 11 Sketch describing the geometry of an emitted wave, the convected wave direction, and the apparent source location after propagation through ambient to translating phased array.

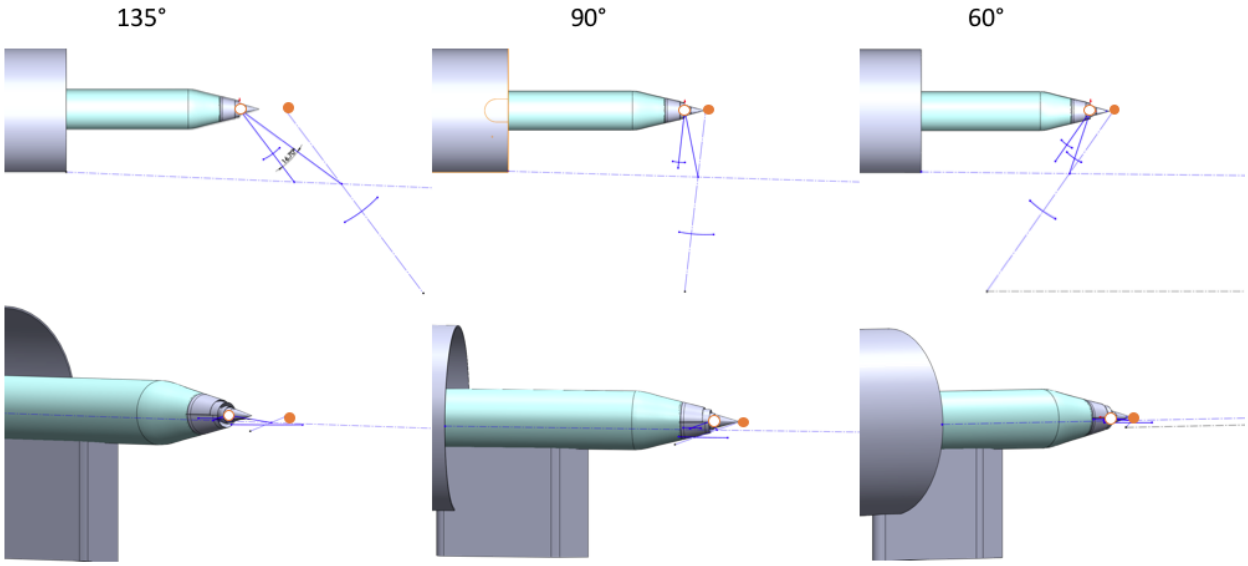

Figure 12 Sketches describing the geometry of the emitted wave, the convected wave, and the apparent source location for observers at 60°, 90°, and 135° for a source located at the nozzle exit in a M_{flight}=0.3 flight stream.

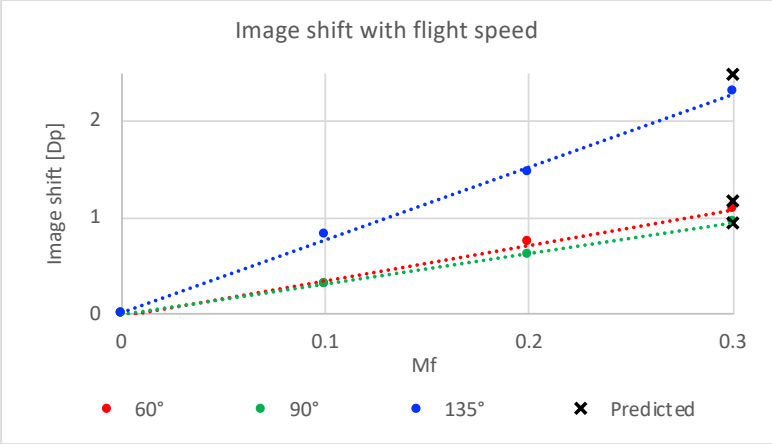

Figure 13 Difference between actual source location and apparent source location from source maps of impinging jet source Black X at Mf = 0.3 are from calculations assuming source at origin and 3° free jet shear layer growth.

Single Stream Jet Beam Forming

Applying the translating phased array to single-stream jets to confirm that the source maps agreed with previous experiments builds confidence in the results. Figure 14 presents the source distribution of the baseline (000B) nozzle with only the primary stream operating, producing an unheated M = 0.98 ($U/c_\infty = 0.9$) jet plume. The figure gives a very detailed look at how the source distributions change with frequency, with maps provided for every 1/3-octave band. The center frequencies are given both in absolute (Hz) and normalized (St) units; the equivalent diameter and fully expanded velocity were used to compute the Strouhal number. Two sources are apparent, one that dominates at low frequencies and shifts upstream with increasing frequency, and another that is spatially locked to the nozzle and dominates at high frequencies. The right side of the figure has the same plots as the left, but with ovals drawn around these two sources for clarity: the pink ovals highlight the moving 'plume' source, while green ovals highlight the 'nozzle-locked' source.

For nozzles without an exposed centerbody (plug), at high frequencies the phased array often picks up the shear layers of the jet. Since the source region here is confined to the center of the jet, on the plug, it is possible that the plug is acting as a reflector for the shear layer sources, making them more like a dipole and hence more efficient. Perhaps this is why the downstream source that moves upstream with frequency and scales well with local length scales is dominated at high frequency by the source at the plug.

Not shown here, the plume source has previously been found to have strong change in amplitude with flight speed while the nozzle-locked source has been nearly independent of flight speed. What has not been shown is whether a clear nozzle-locked source is present in nozzles without a plug or external inner cowl.

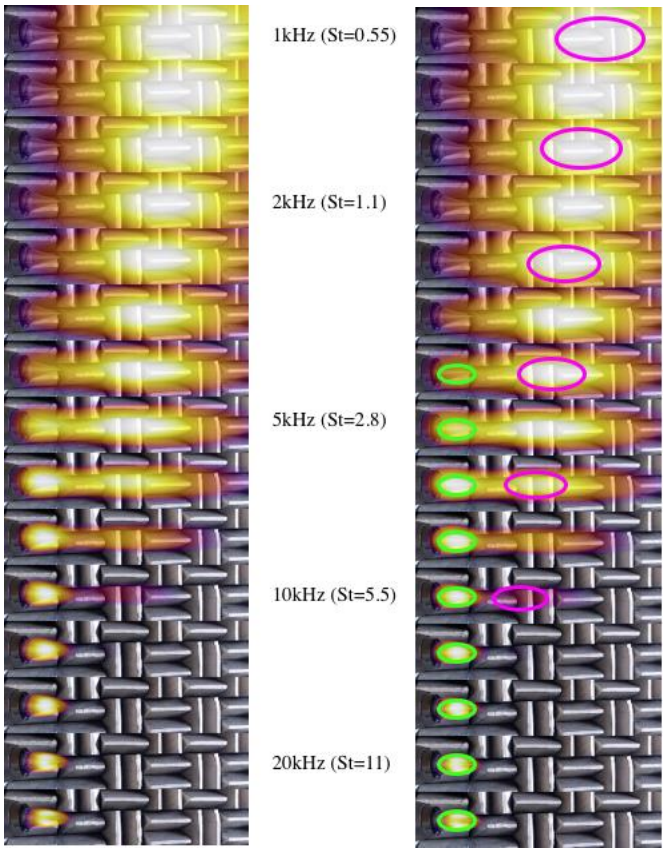

Figure 14 Source distributions as a function of frequency for the baseline (no chevrons/000B) nozzle with flow from primary nozzle only at M= 0.98. Array at 90° to jet axis. Plots on right column have ovals superimposed to highlight 'plume' (pink) and 'nozzle-locked' (green) source regions.

Next we consider how these sources change with polar angle. Figure 15 presents source maps for the same jet flow at five different center frequencies, but from four polar angles (with beamforming to the array normal plane due to the higher accuracy provided). The images have been stretched to correct the perspective so that the source region is scaled in height and length to be the same in all polar angle maps. The contour levels in each plot have been set to the local maximum, which is given numerically in each plot.

One correction not made is for amplitude changes due to distance to true source location, assuming the true source distribution is in the jet plume. These maps were beamformed assuming that the sources were on a plane normal to the array, passing through the jet axis at a point 0.5m (19.7 in) downstream of the plug tip, the center of the phased array field of view for all angles. The low-frequency 'plume' source is near this axial location, so amplitude corrections for angle are not needed for sources in this region. The nozzle-locked sources roughly 0.7m (27.6 in) upstream of the phased array field-center require approximate corrections of -1 dB, 0.5 dB, 1.5 dB, and 1.3 dB for the 60°, 90°, 135°, and 150° angles, respectively. Sources between the phased array field-center and the nozzle would have intermediate corrections.

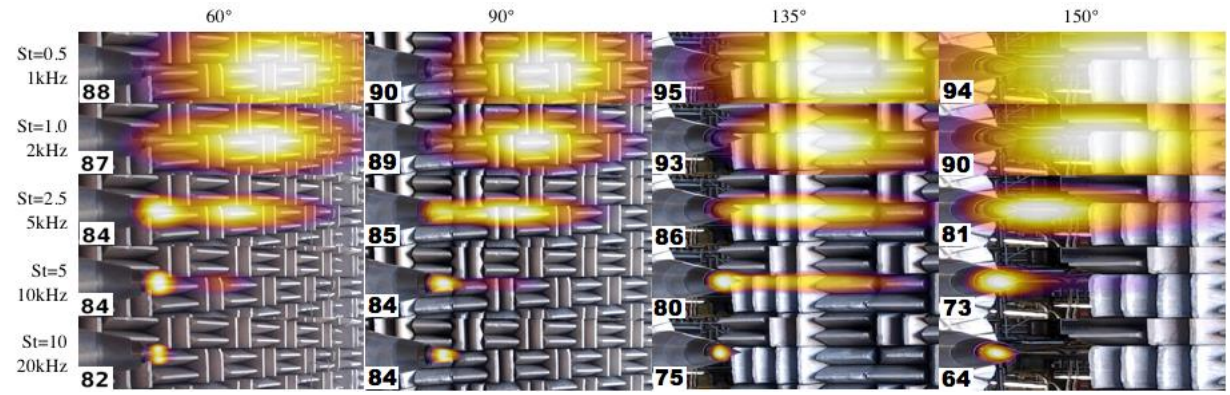

Figure 15 Source distributions for nozzle 000B operating with flow from primary nozzle only at M= 0.98.

Examining the source maps by frequency, the lowest frequency, St=0.5, has the same peak location for all polar angles. The amplitudes are 5 dB higher at the 135° and 150° than at 90° and 7 dB higher than at 60°. This is in keeping with a hypothesis of intrinsic directivity for these plume sources.

As we examine higher frequencies the primary source shifts from the downstream plume source to the upstream nozzle-locked source. At St=2.5 both sources can be distinguished at 90° and 60°. At 135° and 150° the nozzle-locked source cannot be isolated until higher frequencies. This may be due to the viewing angle making distinguishing the sources difficult for the phased array or it may be that the nozzle-locked source is directional and radiates less strongly downstream.

At St=10, the nozzle-locked source is dominant at all angles. Looking closely at 90° and 60°, it appears that this source is located midway down the plug, and appears to have radial extent closer to that of the inner nozzle lip than to the outer nozzle lip. It is also longer axially and stronger in the 90° view than the 60° view. The perception is that the source is associated with the inner shear layer caused by the backward step of the (non-operational) inner nozzle rather than to the outer shear layer of the primary stream.

Effect of Chevrons on Noise Source Distrbution

Nozzles with four different chevron configurations were tested with the phased array: 1) the low penetration chevrons on the lip between the primary and flight streams, 2) the high penetration chevrons on the lip between the primary and flight streams, 3) the low penetration chevrons on the lip between the primary and tertiary streams, and 4) the high penetration chevrons on both sections of the primary stream lip. The nozzle rotation allowed the chevrons to be located on the microphone/observer/near side (designated as A180) or the opposite/far side (designated as A0) of the plug. These tests were performed with the primary stream at M = 1.05, the secondary stream at M=0.95, and the freestream at M=0.3.

Figure 16 shows the difference in far field spectral directivity caused by adding chevrons to the baseline nozzle on the 180° arc between the primary and flight streams. Results are provided for both lower-penetration/100B (part a) and higher-penetration/200B (part b) chevrons located on the far side of the plug (A0). For the lower penetration 100B chevrons, there is a 2 dB increase in sound above 10 kHz for angles forward of 90° and 2-3 dB reduction in frequencies below 2 kHz at almost all angles. The higher penetration chevrons 200B have a 4 dB increase at high frequency and roughly the same 2-3 dB reduction at low frequencies.

The corresponding source maps for the two chevron designs (100B and 200B) are presented in Figure 17, along with the maps for the baseline nozzle (00B) for reference. At 1 kHz, the peak levels of the plume source are essentially the same for all nozzles, but the distributions are shifted upstream by the chevrons with the shift increasing with the increased penetration. The downstream angle shows very little shift, but both the 60° and 90° angles show the source shift significantly. At 10 kHz, the peak levels of the nozzle-locked sources are increased by the chevrons at upstream angles; whereas they remain essentially the same at the 135° angle. There is a slight downstream shift and lengthening of the distributions with the addition of chevrons, but they essentially remain located along the nozzle plug when flightstream convection is accounted for. Interestingly, the 135° angle sees the high frequency sources shifted slightly upstream with the addition of chevrons.

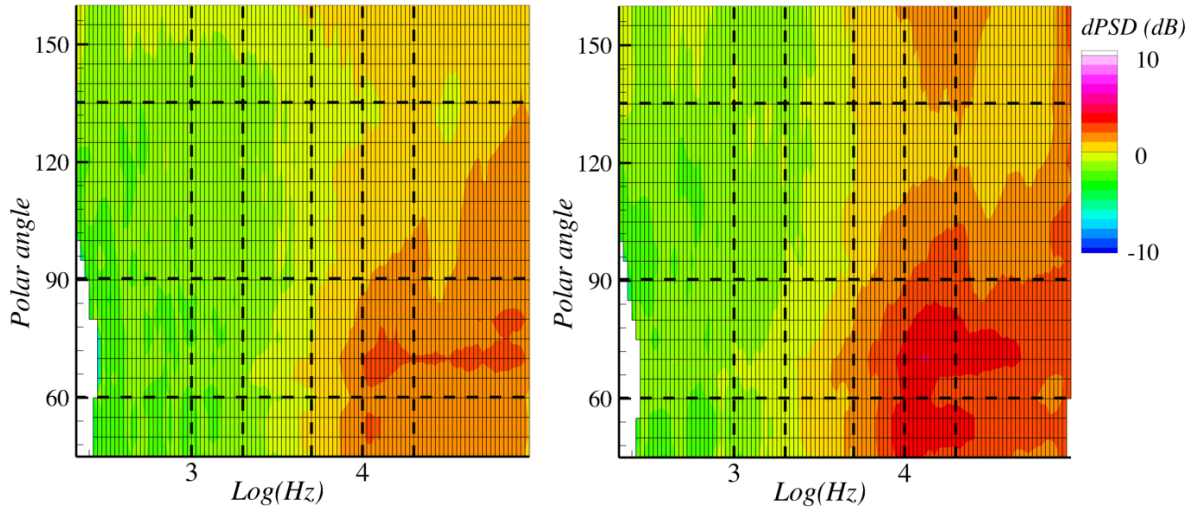

(a) *(b)*

Figure 16 Difference in far field sound directivity caused by addition of chevrons to baseline uninstalled nozzle at Primary M=1.05, Secondary M=0.95, freestream M=0.3. (a) 100B_A0 minus 000B_A0, (b) 200B_A0 minus 000B_A0.

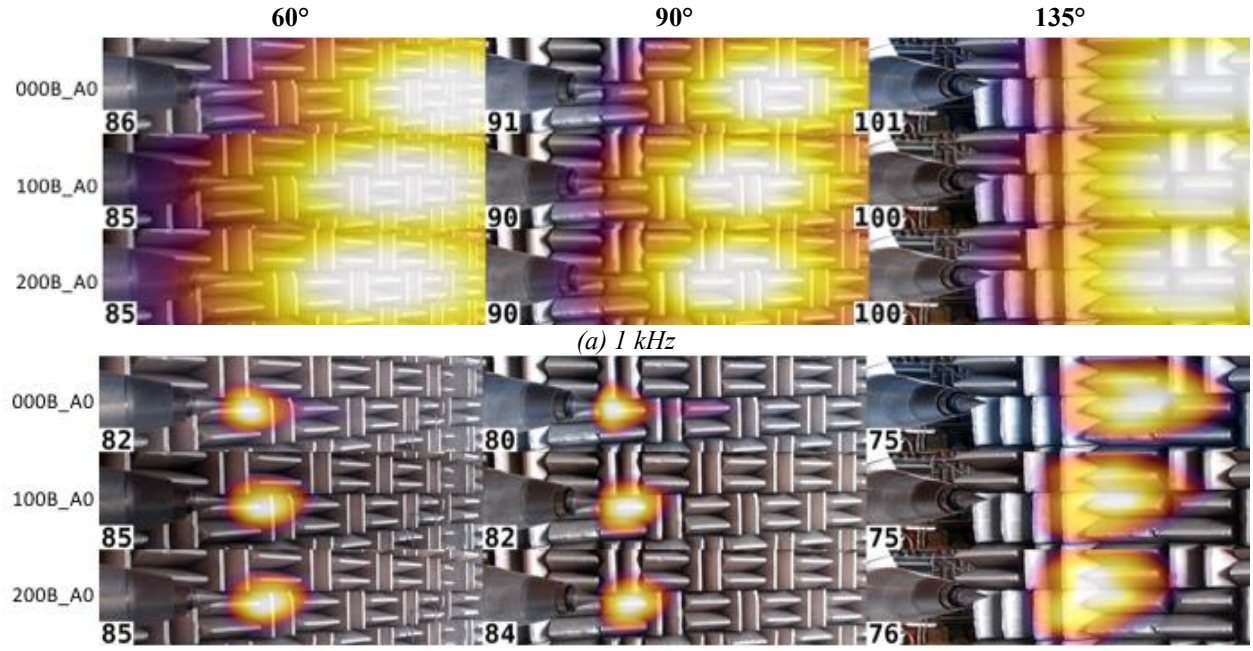

(a) 1 kHz

(b) 10 kHz

Figure 17 Sound source maps for baseline 00B nozzle and chevron nozzles 100B and 200B, at Primary M=1.05, Secondary M=0.95, freestream M=0.3, as viewed from 60°, 90°, and 135°. (a) 1 kHz band, (b) 10 kHz band.

More insight is gained by looking at the source maps corresponding to observers on both sides of a chevron nozzle. Figure 18 shows source maps for the lower-penetration chevrons located on both the far (A0) and near (A180) sides of the plug. At 1 kHz, the source maps on the two sides of the jet are nearly identical, except for a slight reduction in the peak level (2 dB) at the 135° angle associated with having the chevrons on the near side of the plug. At 10 kHz, however, there is a significant noise penalty associated with having the chevrons on the near side of the plug: the peak level is 4, 9, and 11 dB higher at the 60°, 90°, and 135° angles respectively. At the 60° and 90° angles the source location is roughly the same for both sides of the nozzle, but at 135° the source region is much closer to the nozzle when observed from the chevron side. Based on this it seems that the high frequency noise produced by the chevrons is mostly directed toward the observers on the side of the chevrons, not the opposite side.

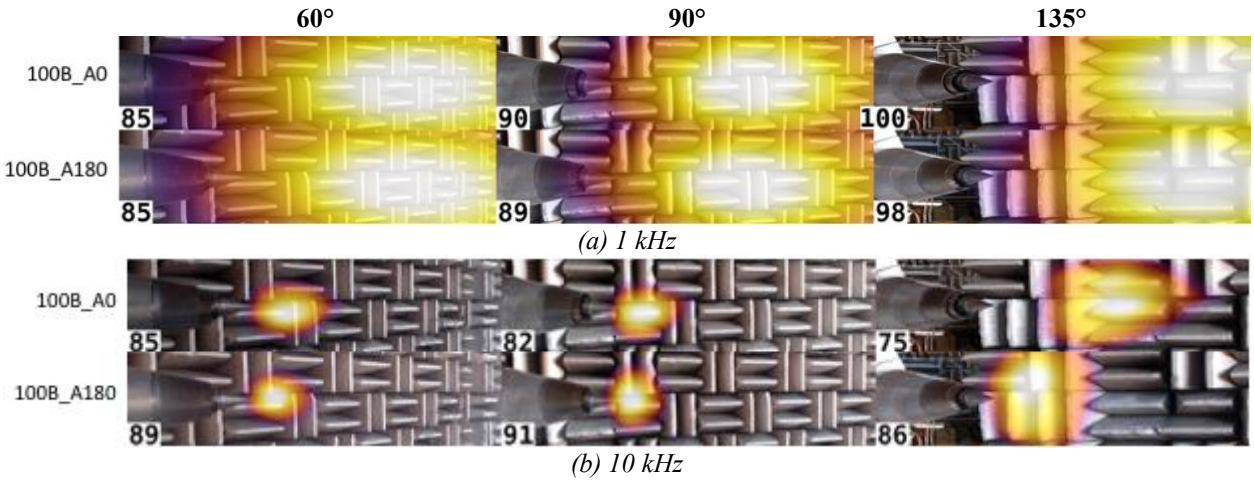

Figure 18 Sound source maps for chevron nozzle 100B with chevrons on side toward (100B_A180) and away from (100B_A0) the observers; Primary M=1.05, Secondary M=0.95, freestream M=0.3. (a) 1 kHz band, (b) 10 kHz band.

The impact of chevrons spectrally is to decrease low frequency, aft-radiated noise and increase high frequency noise, often to broadside and forward angles. The decrease in low frequency noise associated with the addition of chevrons can also be associated with a spatial shift in source location further upstream in the jet for a given frequency. The increased high frequency noise comes from an increase in strength of the nozzle-locked source, which also expands to a larger spatial region. Increasing penetration has little impact on the source maps. At high frequencies, increasing penetration increased peak strength, but not spatial location. The nozzle-locked sources, responsible for the increase in high frequency, radiate preferentially toward the side of the jet with the chevrons, either because they are blocked and/or augmented by the nozzle centerbody, or by intrinsic directivity. The plume source, responsible for the low frequencies impacted by the chevrons, are not as azimuthally directional, being roughly the same to angles on the side with the chevrons or opposite them.

Installation Effects on the Noise Source Distribution

The last objective was to catalog the impact of the installation on the sound sources. Simplistically, because the nozzle plume is far enough from the planform to be relatively undisturbed, the planform should merely shield a portion of the plume, and the phased array would see the remainder of the plume unaffected. PIV measurements indeed showed that the turbulence of the plume for these nozzles was relatively unaffected by the installation on the planform.

To the far field angle directly under the aircraft, the aft deck of the aircraft creates a geometry very similar to that of a wide flat plate. The impact of installing the baseline nozzle above the planform is shown in Figure 19. There is a low-frequency (less than 2 kHz) increase of 3-4 dB at fore and broadside angles. This is countered by a high-frequency reduction in noise of as much as 8 dB at broadside angles.

Phased array maps are shown in Figure 20 for low, medium, and high frequencies to show where these differences are produced. It is important to note that the peak levels of the maps (denoted by the number overlaid on each plot) differ from one another. As shown in part (a), adding the planform tends to increase low frequency (1 kHz) noise emitted in the upstream and broadside directions. To an observer at these locations the peak source location shifts upstream and would be located at the trailing edge of the planform if convection was accounted for. This is consistent with the planform producing a new source that is 3-4 dB louder than the plume source present in both configurations. In keeping with previous findings of this trailing edge source, it has an intrinsic directivity of a dipole oriented normal to the plate. Therefore, it produces little sound to the aft angle and the aft source map is unchanged by installation.

At 5 kHz (part b), the nozzle-locked source is effectively shielded by the planform at 60°. At 90° the nozzle-locked source is shielded, but the slightly louder plume source is unaffected. At aft angles, the distributions look similar, but there was a small reduction in the peak of the source map caused by the installation. At 20 kHz (part c), the nozzle-locked source is shielded so well that the source peak was reduced by 20 dB at 60° and by 11 dB at 90°. The remaining noise distribution appears as a source at the trailing edge of the planform, either because this sound is

produced here or because it is diffracting from upstream sources. Unfortunately, the phased array produced unphysical distributions for both configurations at 135° for this high frequency. In both the baseline uninstalled case and the installed case, however, the beamform peak is very low due to the lack of high frequency directivity in this direction.

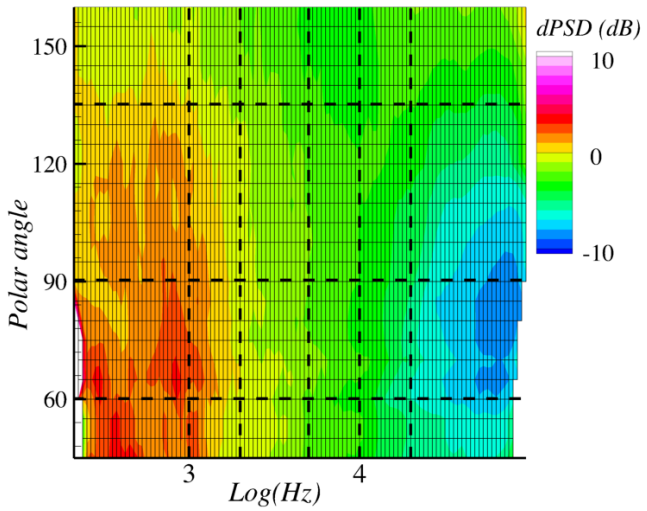

Figure 19 Difference in far field sound directivity caused by installation of baseline nozzle on planform (000T). Difference is 000T_S0 minus 000B_A0, both at Primary M=1.05, Secondary M=0.95, freestream M=0.3.

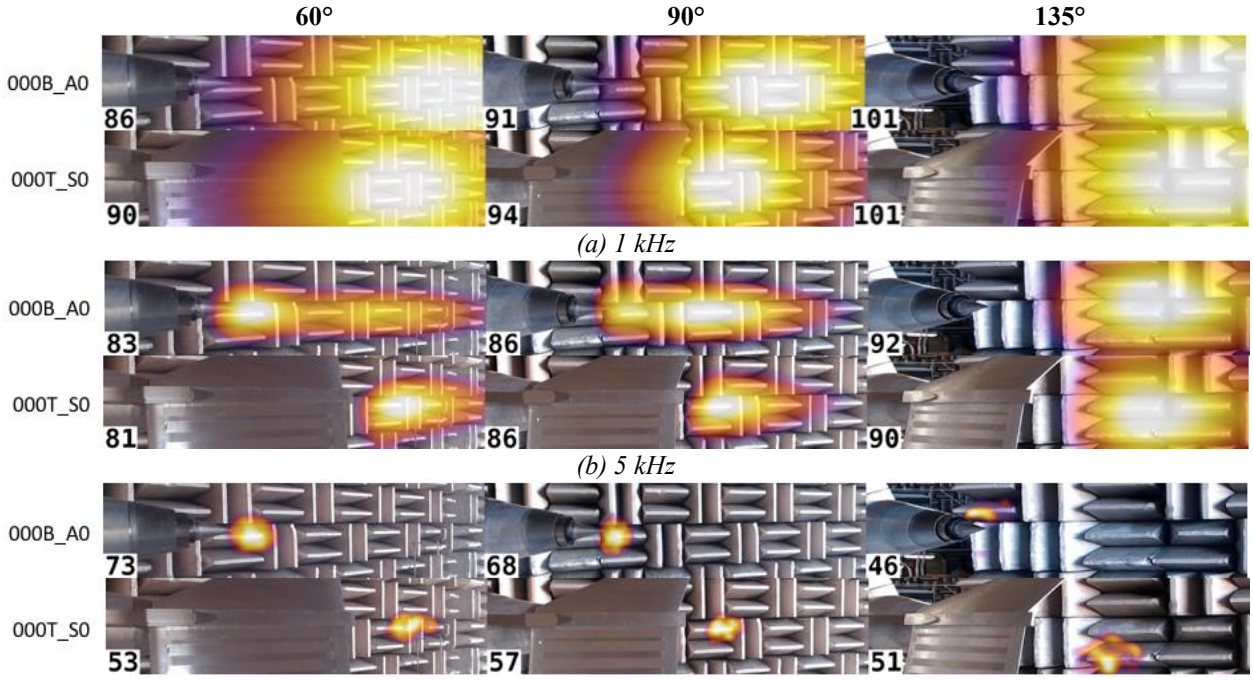

Figure 20 Sound source maps for baseline nozzle, uninstalled (000B_A0) and installed on the planform as observed directly under the aircraft (000T_S0), at Primary M=1.05, Secondary M=0.95, freestream M=0.3, for polar angles 60°, 90°, and 135°. (a) 1 kHz band, (b) 5 kHz band, (c) 20 kHz band.

At the lateral certification position, the planform, which represents partly aft deck and partly tailfin, is between the plume and the observer but the leading edge is farther downstream, potentially shielding the nozzle-locked source less. Figure 21 shows 20 kHz source maps for the baseline nozzle, uninstalled and installed as seen at the lateral angle. Immediately obvious is the source at the leading edge of the tailfin for the 60° angle. The peak level is 9 dB below that of the uninstalled source. At 90°, there is a small diffracted source on the tailfin leading edge more than

12 dB below the unshielded source. At 135° there appear to be strong sources along the leading edge of the planform, but the pattern of the main peak make the beamforming suspect. It is clear, however, that the tailfin is not providing nearly as much shielding as the aft deck for the 60° angle, explaining the reduced benefit of installation for observers to the sides of the notional aircraft.

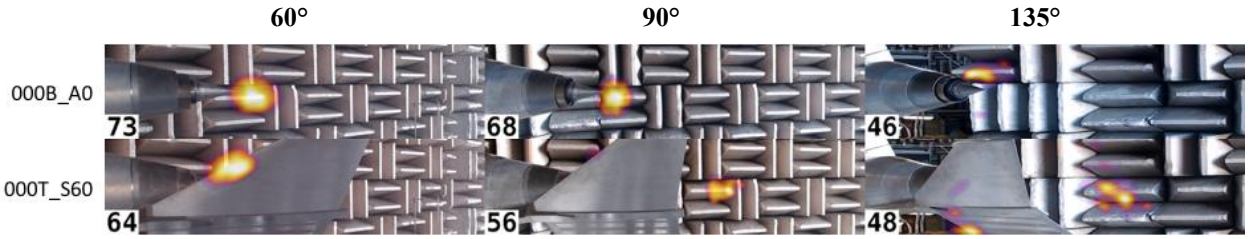

Figure 21 Sound source maps for baseline nozzle, uninstalled (000B_A0) and installed on the planform as observed on a lateral sideline of the aircraft (000T_S60), at Primary M=1.05, Secondary M=0.95, freestream M=0.3, for polar angles 60°, 90°, and 135°. 20 kHz band.

Next, consider the impact of installation on a chevron nozzle, nozzle 040B. The 040B chevrons have the same penetration (high) as the 200B, but are positioned between the primary and tertiary streams (i.e. the same side as tertiary stream). Chevrons tend to move sources upstream, increasing the strength of the high-frequency nozzle-locked source, and decreasing the strength of the low-frequency plume source.

The impact of installation on the spectral directivity of a chevron nozzle can be seen in Figure 22. At broadside polar angles, installation reduces noise over most frequencies above 1 kHz (especially at very high frequency), and produces an increase at low frequencies. Compared with the baseline nozzle (Figure 19), there is more reduction at mid and high frequencies, and possibly less trailing-edge dipole noise.

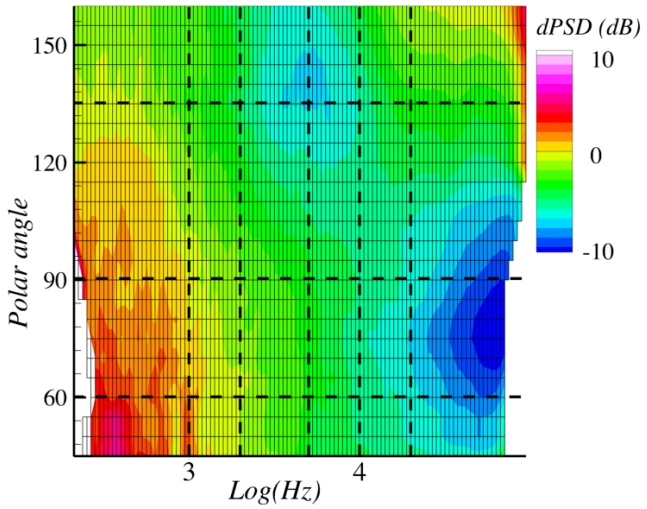

Figure 22 Difference in far field sound directivity caused by installation of chevron nozzle 040B on the planform (040T). Difference is 040T_S0 minus 040B_A0, both at Primary M=1.05, Secondary M=0.95, freestream M=0.3.

Looking at the source maps of the 040 chevron nozzle (Figure 23), uninstalled and installed, and comparing them with the maps for the baseline nozzle (Figure 20), there is less difference in peak levels at low frequency (1 kHz), even though the uninstalled peak of the chevron nozzle is already lower than the baseline nozzle. This implies that the additional trailing edge dipole, while still present, is much weaker for the chevron nozzle. At mid frequencies (5 kHz) the uninstalled source for the chevron nozzle is greater than the baseline nozzle, but the shielding is also much greater, resulting in 1-2 dB reduction in peak source strength. Significant shielding occurs even at the 135° polar angle. At 20 kHz, the impact of installation on peak source strength at 15-30 dB, with no sign of sound being diffracted around the leading or side edges of the planform.

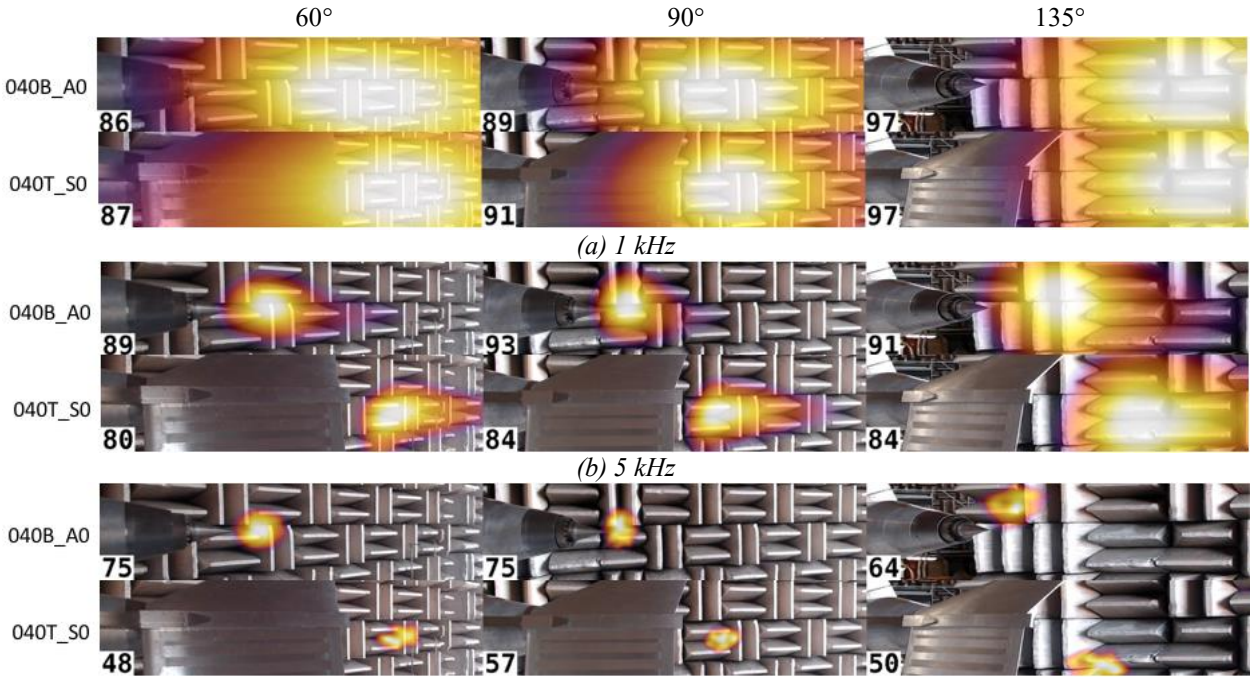

(a) 1 kHz

(b) 5 kHz

(c) 20 kHz

Figure 23 Sound source maps for chevron nozzle 040B, uninstalled (040B_A0) and installed on the planform as observed directly under the aircraft (040T_S0), at Primary M=1.05, Secondary M=0.95, freestream M=0.3, for polar angles 60°, 90°, and 135°. (a) 1 kHz band, (b) 5 kHz band, (c) 20 kHz band.

VI. Summary

Phased array data were acquired on a series of nozzles with different chevron designs, both uninstalled and installed at NASA Glenn's Aero-Acoustic Propulsion Lab. The data were processed to explore the impact of chevrons and installation effects on the noise source distribution as well as to evaluate the new translating phased array.

The operation of the phased array was validated during this test and several operating modes were tested. These include several different beamforming algorithms, of which Functional Beamforming appeared to yield the most consistent results. Additionally, an attempt was made to project results from different polar angles onto the same plane for more direct comparison. This process was found to not be accurate enough with data at this resolution leading to incorrectly positioned noise sources. As a result, beamforming was limited to regions of interest parallel to the plane of the array.

Additionally, the impact of the free jet flow on the beamforming results was explored and a simple model was developed that predicts the downstream shift in noise source location caused by convection. This model, based on array angle and free jet velocity, closely matched the observed behavior and will allow for corrections to be integrated into future processing.

Beamforming was performed on a simple single-stream jet in order to compare with previous research. The current results agree with the previous findings for externally mixed nozzles containing an external plug. Two general source regions were found: an extended 'plume' source that dominates at low frequencies and moves from downstream to upstream with increasing frequency, and a 'nozzle-locked' source that dominates at high frequencies but stays spatially locked to the a region just downstream of the nozzle exit on the side of the plug. In general, the two-source structure was observed from all polar angles, although at the far-downstream angle it was difficult to distinguish both because of the viewing angle.

Lastly, the effect of installation on sound sources was examined and was largely as predicted. Sources near the nozzle are shielded at upstream and broadside angles by as much as 20 dB via the planform. Low frequencies downstream appear to be unaffected, but this is difficult to accurately assess because the planform creates a new low frequency source at its trailing edge that is usually higher than the jet mixing noise. When chevrons are applied to

the nozzle and sources are moved upstream, the shielding of the planform becomes more effective. However, with increased penetration comes increased high frequency source strength, and the effect of shielding is limited. This is especially true for angles at the lateral position, where the planform is not as effective at shielding and sound is diffracted around the tailfin and other edges.

Acknowledgements

This work was supported by the Commercial Supersonic Technology Project of the Advanced Air Vehicles Program at NASA. The excellent data were made possible by a highly skilled team of engineers and technicians at NASA Glenn's Aero-Acoustic Propulsion Lab.

References

[1] Bridges, J. E., "Aeroacoustic Validation of Installed Low Noise Propulsion for NASA's N+2 Supersonic Airliner," *2018 AIAA Aerospace Sciences Meeting*, Kissimmee, Florida: American Institute of Aeronautics and Astronautics, 2018.

[2] Morgenstern, J., Buonanno, M., Martin, L., Yao, J., Murugappan, M., Paliath, U., Cheung, L., Malcevic, I., Ramakrishnan, K., Pastouchenko, N., Wood, T., Martens, S., Viars, P., Tersmette, T., Lee, J., Simmons, R., Plybon, D., Aviation, G., Alonso, J., Palacios, F., Lukaczyk, T., and Carrier, G., "Advanced Concept Studies for Supersonic Commercial Transports Entering Service in the 2018-2020 Period Phase 2," *New York*, 2015, p. 396.

[3] Bridges, J., "Noise measurements of a low-noise top-mounted propulsion installation for a supersonic airliner," *AIAA SciTech Forum 2019*, American Institute of Aeronautics and Astronautics, 2019.

[4] Bridges, J. E., and Wernet, M. P., "PIV measurements of a low-noise top-mounted propulsion installation for a supersonic airliner," *AIAA SciTech Forum 2019*, American Institute of Aeronautics and Astronautics, 2019.

[5] Heberling, B. C., "Numerical Investigation of a Shielded Chevron Nozzle," *AIAA SciTech 2019*, American Institute of Aeronautics and Astronautics, 2019.

[6] Dougherty, R. P., "Functional Beamforming for Aeroacoustic Source Distributions," *20th AIAA/CEAS Aeroacoustics Conference*, Atlanta, GA: American Institute of Aeronautics and Astronautics, 2014.

[7] Bridges, J., Brown, C. A., and Seidel, J. A., "NASA's Pursuit of Low-Noise Propulsion for Low-Boom Commercial Supersonic Vehicles," *54th AIAA Aerospace Sciences Meeting*, 2018.